Solar Energy Materials and Solar Cells 170 (2017) 77–86

Contents lists available at ScienceDirect

Solar Energy Materials and Solar Cells

journal homepage: www.elsevier.com/locate/solmat

Corrosion behavior of Ni-based alloys in molten NaCl-$CaCl_2$-$MgCl_2$ eutectic salt for concentrating solar power

Bo Liu[a], Xiaolan Wei[a], Weilong Wang[b,*], Jianfeng Lu[b], Jing Ding[b]

[a] School of Chemistry and Chemical Engineering, South China University of Technology, Guangzhou 510640, PR China
[b] School of Engineering, Sun Yat-sen University, Guangzhou High Education Mega Center, Guangzhou 510006, PR China

ARTICLE INFO

Keywords:
Chloride molten salt
High temperature corrosion
Inconel 625
Hastelloy X, Hastelloy B-3

ABSTRACT

In this work, the corrosion behavior of Ni-based alloys including Inconel 625(In625), Hastelloy X(H X) and Hastelloy B-3(H B-3) alloys were investigated in a molten salt NaCl-$CaCl_2$-$MgCl_2$ by gravimetric methods. The corrosion test was conducted at 600 °C for a maximum immersion time of 3 weeks. The corrosion behavior was determined by measuring the mass loss of samples at different time intervals. The corrosion products and morphology were investigated in detail via X-ray diffraction (XRD) and scanning electron microscope (SEM). The microscopic area element analysis in corrosion surface and the mapping diagram of element distribution from corrosion profile were carried out by energy dispersive spectroscopy (EDS). The results show that In625 alloy resists corrosion better than H X and H B-3 alloys in molten salt NaCl-$CaCl_2$-$MgCl_2$ in the presence of air. The corrosion profile in In625 and H X alloy show a poor Cr zone in the inner corrosion layer, probably caused through the outward diffusion of $CrCl_4$(g) which is forecasted the formation by thermodynamic calculation. $MgCr_2O_4$ attached to the In625 and H X alloys specimens surface formed a compact protective layer and thus resist corrosion well. Thin and uniform corrosion layer was observed from profile in H B-3 alloy after immersed in NaCl-$CaCl_2$-$MgCl_2$ molten salt when air was present, however there is not a poor Cr zone in corrosion profile of H B-3 alloy. From above, the corrosion rate of Ni and Mo in alloy dominates the corrosion rate. Certain amount of Cr in the nickel-based alloys enhanced its corrosion resistance in molten salt NaCl-$CaCl_2$-$MgCl_2$, even if Ni and Mo in nickel-based alloys shows more stable performance in the corrosion test in chloride molten salt.

1. Introduction

Concentrating solar power (CSP) is an emerging sustainable technology for power generation. The sunlight is concentrated to heat the heat transfer fluid (HTF), which is then pumped to a heat exchanger to generate steam to drive steam turbines for power production. HTF is one of the most important components for overall performance and efficiency of the CSP system. Current CSP plants use nitrate molten salts as HTFs and can operate with multiple hours of energy storage capacity. Next-generation of solar power conversion system in CSP application are targeting high-temperature, advanced fluids to be operated at the range of 600–800 °C, which exceeds the stability temperature of nitrate [1]. At the higher operating temperatures achievable in solar power tower-type CSP plants, chloride salts are promising candidates for application as thermal energy storage materials, owing to their thermal stability and generally low cost [2]. Ionic metal chloride salts, such as NaCl, $CaCl_2$, $MgCl_2$, KCl are abundant in nature and boil at temperature higher than 1400 °C. As a class of potential high temperature heat transfer fluid, NaCl-$CaCl_2$-$MgCl_2$ eutectic system shows the advantages of low cost, great heat storage temperature range, super heat of fusion, low viscosity and good thermal stability [3]. However, molten chlorite has a sharp corrosive action on container and piping alloys in the CSP system [4]. Corrosion is a major problem in the CSP system, especially under high temperature operating condition [2].

There are several reports available on corrosion issue of chloride salt mixtures. The corrosion behavior and mechanisms of pure nickel (Ni), GH4033 and GH4169 in 793 K molten eutectic NaCl-$MgCl_2$ were studied by Jun-wei Wang et al. [4]. They reported that the corrosion resistance of pure Ni is better than GH4033 and GH4169. The Cr and Fe elements in the alloys would preferential oxidization and chlorination. After comparing the corrosion of the alloys with different Cr content in the chloride salts, Manohar S. Sohal points out that increasing Cr content increased the rate of corrosion, while changes in nickel content seemed to have no effect [5]. Also, it has been reported that Cr is not an effective element for improving corrosion resistance of Fe-based and Ni-based alloys. Because Cr_2O_3 has a higher solubility than iron and nickel oxides, it will react more readily with chloride salt [6,7]. However, K. Vignarooban et al. [8] have studied the corrosion resistance of

* Corresponding author.
E-mail addresses: wwlong@mail.sysu.edu.cn (W. Wang), dingjing@mail.sysu.edu.cn (J. Ding).

http://dx.doi.org/10.1016/j.solmat.2017.05.050
Received 2 January 2017; Received in revised form 1 May 2017; Accepted 20 May 2017
Available online 01 June 2017

Hastelloys C-276, C-22 and N types in eutectic molten salts containing NaCl, KCl and $ZnCl_2$ and found that Hastelloys N showed higher corrosion rates than C-276 and C-22, even though Hastelloy N has higher nickel content. Hastelloy N is more susceptible for increased corrosion, because Hastelloy N has lower Cr content (7%) compared to C-276 and C-22. The effect of the elements on the corrosion resistance of the alloy remains to be studied. In addition, by using electrochemical method, Inconel 625 was reported as the most corrosion-resistant alloy in molten 34.42NaCl-65.58LiCl (wt%) at 650 °C, with a corrosion rate of 2.80 ± 0.38 mm/year in a nitrogen atmosphere than SS347, SS310, and Incoloy 800 H [1]. These alloys exhibited localized corrosion. In the presence of oxygen, the alloy forms oxides that eventually dissolve into the molten chloride salt liberating the oxygen component which then later is able to keep the oxidization process going. Intergranular corrosion is the major corrosion type found in alloys exposed to molten chlorides in oxidizing atmosphere [9]. Shunv Liu et al. [10] have studied the isothermal corrosion of TP347H, C22 alloy and laser-cladding C22 coating in molten alkali chloride salts at 450–750 °C. At lower test temperatures, chemical corrosion plays a dominated role. The corrosion mechanism involves accelerated oxidation of alloys by gaseous Cl^-/Cl-species, which is often referred to as active oxidation. At higher test temperatures, electrochemical corrosion plays a dominated role. The corrosion may be further enhanced if the protective surface oxide scale is dissolved by molten salts. Under this circumstance, accelerated corrosion happens for oxygen as well as other aggressive media can still access to the fresh alloy and diffuse in the alloy substrate.

It have been reported that the corrosion rate of the nickel-based alloys was found to increase with increasing partial pressure of oxygen [11]. Water vapor also could play a role in the corrosion process [2]. Atmospheric air plays a big role in inducing the corrosion in molten-salt/alloy systems [12]. Thus, in a non-inert environment, the effect of water vapor and oxygen in the air and molten salts on the corrosion of molten salt / alloy systems should be taken into account.

However, there are few reports available on corrosion issues of alloys in contact with molten eutectic NaCl-$CaCl_2$-$MgCl_2$. The corrosion mechanism is not clear yet. Corrosion characteristics of the elements in the alloys in the molten salt under low oxygen partial pressure also need to be studied.

Nickel-based alloys are widely used in industry under aggressive conditions owing to their perfect corrosion resistance [13–15]. Therefore, nickel-based alloys are frequently employed in corrosive applications. In this study, Inconel 625, Hastelloy X and Hastelloy B-3 alloys were chosen as research subjects.

The corrosion behaviors of Inconel 625, Hastelloy X and Hastelloy B-3 alloys in thermal storage medium of molten eutectic NaCl-$CaCl_2$-$MgCl_2$ has scarcely been reported in the literature. Therefore, this paper aims to investigate the corrosion of Inconel 625, Hastelloy X and Hastelloy B-3 alloys in eutectic NaCl-$CaCl_2$-$MgCl_2$ at 600 °C with low oxygen partial pressure. Corrosion behavior was investigated based on the changes in mass and analyses of chemical composition and microstructure of specimens following induced corrosion.

2. Experimental

2.1. Materials

The NaCl, $MgCl_2$ and $CaCl_2$ were purchased from Alfa Aesar for making the ternary eutectic mixture with a melting point of 425 °C for a composition of 53.43,14.95 and 31.61 mol% [3]. All the salts used in this study were stored in inert atmosphere or under vacuum before loading them into the furnace where the salt mixture was heated above 200 °C within 30 min since there was little bulk water. Then the mixtures were heated to 600 °C, held for 3 h to ensure a homogeneous mixture and then cooled to ambient temperature. The solidified salt mixture was ground into power using mechanical rolling, sealed in sample bags and kept in desiccators. These steps were carried out in an isolated air environment.

Table 1
Main composition of the samples (wt%).

Alloy	Cr	Fe	Ni	Mo	Mn	W	Si	Other
Inconel625	22.85	3.41	59.7	8.6	0.089	0.08	0.176	Nb + Ta 3.65
Hastelloy X	22	18	47	9	-	-	-	Co 1, W 0.5
Hastelloy B-3	1.5	1.5	65	28.5	0.595	3.00	0.01	Co ≤ 3.00

All the alloys used in this experiment were purchased from GoodFellow. The alloys composition is shown in Table 1. The specimens of Inconel 625(In625), Hastelloy X(H X) and Hastelloy B-3(H B-3) alloys in the gravimetric corrosion test were cut to the dimension of 30 mm × 15 mm × 2 mm. The specimens were polished by 400, 800 and 1200 grit emery paper in turn and then with diamond paste to obtain a mirror-like finish for corrosion testing, followed by washing and cleaning with water and acetone. After being dried, the sample dimensions were measured with an electronic caliber and weighed with an analytical balance with an accuracy of 0.00001 g.

2.2. Corrosion experimental procedure

The isothermal corrosion was carried out in air atmosphere using a muffle furnace at 600 °C. The specimens were completely immersed in 12 covered alumina crucibles, which contained the mixture NaCl-$CaCl_2$-$MgCl_2$. The 12 covered alumina crucibles was numbered 1–12. Among them, No.1 to No.4, No.6 to No.9 and No.11 crucibles was placed only one piece of alloy, three pieces of alloys were placed in No.5, No.10 and No.12 crucibles, respectively. Remove the crucible from the furnace every 1 day until No.10, and then remove crucibles No.11 and No.12 on days 14 and 21. After the immersion tests, the specimens were taken out of the muffle furnace and cooled together with the molten salt to room temperature to avoid oxidation. The post-corrosion treatment was carried out to one piece of alloy in alumina crucibles No.1 to No.12 according to the standard method described in ASTM G1-03 [16]. The mass loss and corrosion rate curves of the alloy was calculated.

The Eq.(1) for calculating the mass loss over time is [17]:

$$\frac{\Delta m}{S_0} = \frac{m_i - m_f}{S_0} \tag{1}$$

where m_i is the initial mass of the specimen in gram, m_f is the mass of this specimen at time t in gram, and S_0 is the initial area of the specimen in cm^2.

The corrosion rate (CR) values were calculated using the following equation [18], assuming uniform dissolution:

$$CR(\mu m/y) = (365) \cdot 10000[\Delta m/(\rho \cdot S \cdot T)] \tag{2}$$

where $\triangle m$ is the weight loss in gram, ρ is density(g cm^{-3}) of the alloy, S is the total immersed area in cm^2,T is the immersion duration in days.

After ultrasonic washing and drying, the other two pieces of alloys in the crucibles No.5, No.10 and No.21 would be used for XRD analysis and SEM observation.

2.3. Analysis method

The surface and cross section morphology of specimens after corrosion were observed by scanning electron microscope (SEM). Specimens were prepared for cross-sectional metallographic examination using standard grinding and polishing procedures. The specimens were coated with organic polymer materials to avoid damaging the corrosion products on the surface of the specimens during the sample preparation. Energy dispersive spectroscopy (EDS) was used to analyze the chemical composition of the specimens. The crystallographic structures of the corrosion products on the surfaces of the specimens

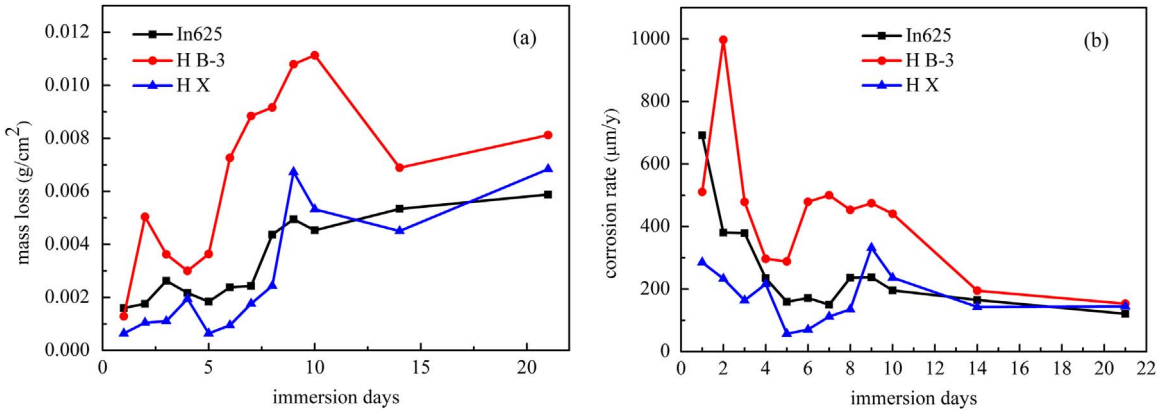

Fig. 1. Mass loss ($\triangle m/S_0$) (a) and corrosion rate (b) of In625, H X and H B-3 alloys after 21 days immersion at 600 °C.

were analyzed using X-ray diffraction (XRD).

3. Results and discussion

3.1. Corrosion performance of alloy specimens in molten salt

The mass change plots can give an indication for the mechanism of corrosion [19]. The gravimetric mass change for In625, H X and H B-3 in molten salt NaCl-$CaCl_2$-$MgCl_2$ at 600 °C are shown in Fig. 1(a). All alloys specimens showed a decrease in mass. Mass loss with immersion time presents an irregular growth initially, and then a rapid increase at the middle stage, finally tends to be stable. This indicates that the growth of corrosion products is controlled by solid state diffusion growth process which provides the protective behavior and the corrosion products have a limited rate of dissolution in molten salt. The mass loss of In625, H X and H B-3 alloys tended to be stable at 5 mg/cm^2, 6.3 mg/cm^2 and 8 mg/cm^2.

The corrosion rates, being calculated from the descaled mass loss of alloy specimens are shown in Fig. 1(b). Under the experimental conditions, In625, H X and H B-3 alloy specimens are corroded severely. After 21 days immersion, the corrosion rate values of In625, H X and H B-3 alloys saturates at around 121.09 μm/y, 153.16 μm/y and 144.59 μm/y, respectively. Since the experiments were carried out in air atmosphere, it was obviously that the water vapor and oxygen in the air had a significant effect on corrosion.

As seen in Fig. 1, In625 and H X alloys show a better corrosion resistance than H B-3 alloy in molten NaCl-$CaCl_2$-$MgCl_2$ eutectic salt at 600 °C. According to Table 1, H B-3 alloy has a higher Ni, Mo content than In625 alloy. However, the content of Cr in H B-3 is much lower than that of the In625 alloy. Previous research has shown that, the selective oxidation of Cr and Mo, and the preferential dissolution of Cr_2O_3 and MoO_2 by molten chlorides left a NiO skeleton, which contributes to the better corrosion resistance of C22 alloy in a mixture of KCl-NaCl [10]. High content Mo and low content Cr in Hastelloy C-276 alloy were considered to be responsible for the better anti-corrosive performance in molten FLiNaK salt by Min Liu et al. [20]. To explain this behavior, XRD analysis and surface SEM imaging was performed.

3.2. Corrosion products and corrosion morphology

The surface morphologies of In625(a), H X(b) and H B-3(c) alloys specimens after 5(1), 10(2) and 21(3) days immersion in molten NaCl-$CaCl_2$-$MgCl_2$ eutectic salt at 600 °C are presented in Fig. 2, respectively. After 5 days immersion, the surface of the specimens all showed a porous morphology. But the size of pores on H X alloy surface is larger than that of In625 and H B-3 alloys. Some cracks are observed on the surface of H B-3 alloy, particularly. The surfaces of the alloys all becomes more uneven after 10 days immersion. The cracks on the surface of H B-3 alloy become more intensive (Fig. 2(c_2)), too. After 21 days immersion, many particles are observed on the superficial image of In625 alloy (Fig. 2(a_3)). The layer under the particles is compact and flat. The surface of H X alloy showed a uniform but still porous morphology after 21 days immersion (Fig. 2(b_3)). After 21 days immersion , the surfaces of H B-3 alloy become uneven with many convex structure (Fig. 2(c_3)). The Figures clearly depict the pore size gets enlarged with increase in the duration of exposure.

Fig. 3 shows these features more clearly at a higher magnification. The EDS analysis results of the corresponding regions on the specimens' surface are shown in Table 2. Comparing the chemical composition of the non-corroded In625 alloy (Table 1) with the regions analyzed after 5 days corrosion (Fig. 3(a_1)), the EDS of the corroded surface showed chromium depletion and a lower iron content at the alloy's surface. O and Mg is also detected on the alloy surface (Table 2(Region 1)). After 10 days corrosion, the surface of the alloy is characterized by different regions of enriched (O, Cr, Mg) and (O, Ni) (Table 2(Region 2, 3)). According to EDS results (Table 2), the observed particles on the surface of In625 after 21 days corrosion test mainly contain (Ni, O, Mo) (Table 2(Region 4)). The layer under the convex particles rich in O, Cr and Mg (Table 2(Region 5)).

A multi-layered corrosion scale appears on the surface of H X alloy after 5 days immersion (Fig. 2(b_1)). According to EDS results, the Cr and O content in the outer corrosion product layer (Region 7) is lower than in the inner layer (Region 6). The analyzed region in Fig. 2(Region 7) shows Cr and Fe depletion with a certain amounts of Mo, very high Ni content, and the presence of O. The region analyzed in Fig. 2(Region 6) exhibits a (O, Mg, Cr)-rich layer. The Fe content in both of the corrosion product layer are very low. After 10 days of corrosion, an enriched in Ni with small amounts of Fe and Cr layer is detected on the surface of H X alloy (Table 2(8, 9)). According to the EDS results, (O, Mg, Cr)-rich compositions are identified as major phases in the corrosion products after 21 days immersion.

Comparing the chemical composition of the non-corroded H B-3 alloy (Table 1) with the regions analyzed after 5, 10 and 21 days corrosion (Fig. 3(c_1, c_2)), the EDS of the corroded surface also showed Cr and Fe depletion at the alloy's surface even the content of Cr and Fe in non-corroded H B-3 alloy is relatively low. After 5 days corrosion, the content of Ni and Mo on the surface of the alloy do not change much. After 10 days immersion, Mg is detected on the alloy surface (Table 2(Region 13, 14)). The content of Ni and Mo on the surface of H B-3 alloy decreases with the increase of O and Mg content. After corrosion for 21 days, the content of O on the surface of H B-3 alloy is relatively high, and the (Ni, O, Mg)-rich compositions are identified as major phase in the corrosion products.

According to reports [10], the formed dense oxide scale composed of Cr_2O_3, NiO and Fe_3O_4 can provide protection for the substrate alloy from further attack by covering the surface of substrate. This indicates

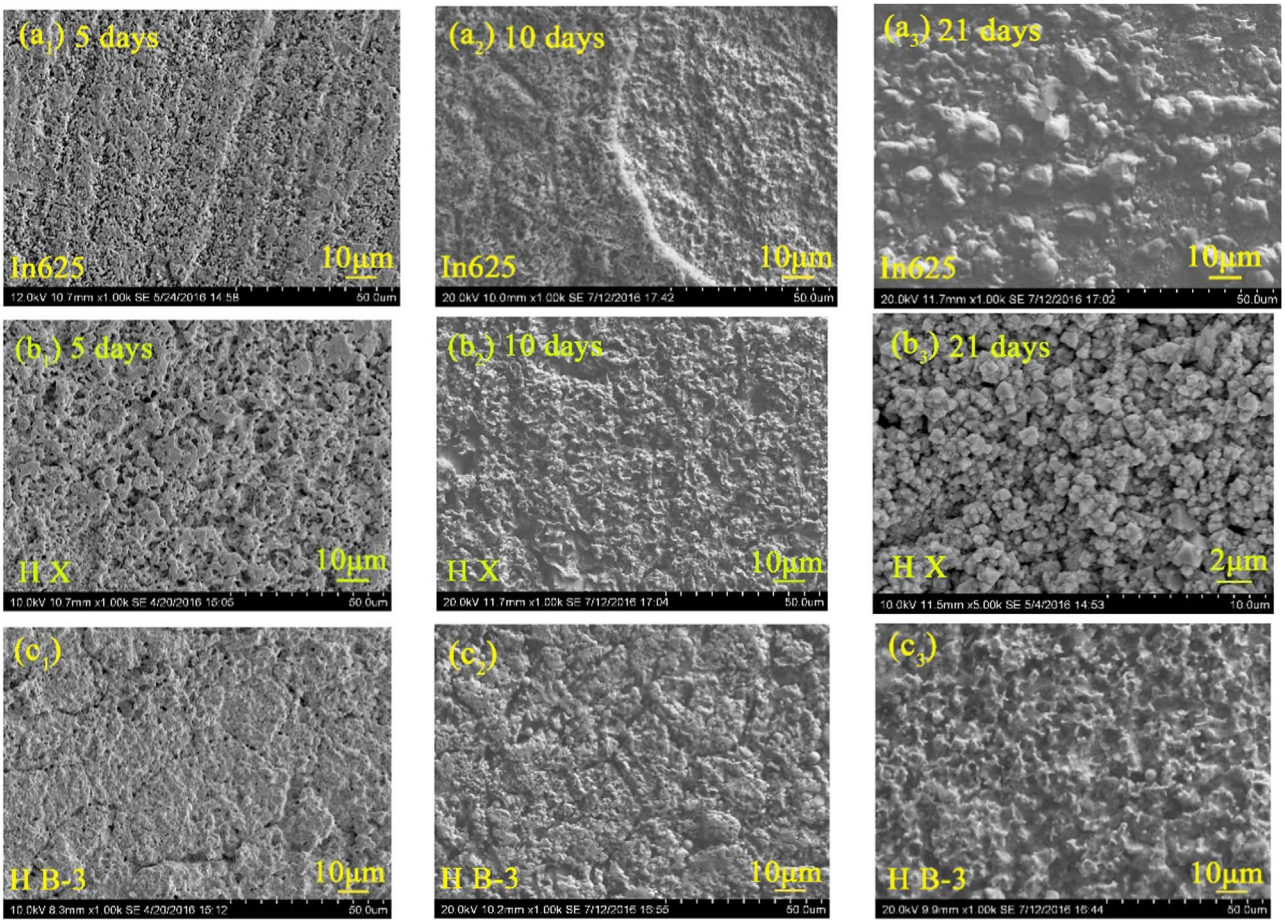

Fig. 2. Surface morphologies of specimens after 5(1), 10(2) and 21(3) days immersion: (a) In625, (b) H X and (c) H B-3.

that the surface protective Cr_2O_3 and Fe_3O_4 scale on the surface of In625 and H X alloys may be destroyed after 5 days immersion. The corrosion media can permeate inwards to corrode substrate alloy. However, after 21 days immersion, it seems that a new relatively dense corrosion layer formed on the surface of the alloys which has a protective effect for the substrate alloy from further attack by covering the surface of substrate. For H B-3 alloy, containing less Fe and Cr, the surface of the alloy still uneven and have many pores and convex structures after 21 days corrosion. It is good for the corrosion media permeate inwards to corrode substrate alloy.

The X-ray diffraction patterns of corrosion products covered the surfaces of In625, H X and H B-3 alloys specimens after corrosion for 0, 5, 10 and 21 days are presented in Fig. 4(a), (b) and (c), respectively. The phase of Cr0.19Fe0.7Ni0.11 is detected to be the substrate phase both of the In625 and H X alloys. But the phase of the specimens' substrate of In625 and H X alloys on the surface has changed from the original Cr0.19Fe0.7Ni0.11 into Ni2.9Cr0.7Fe0.36 with the increase of immersion time. This indicates that the Fe and Cr have lost from the surface of the specimens with the increasing immersion time which is consistent with the EDS analysis results of the alloy surface (Table 2). After 10 days immersion, $MgCr_2O_4$ peaks are identified on the surface of In625 alloy. $MgCr_2O_4$ and NiO are the major phases on In625 alloy after 21 days immersion, in addition to the phase of the specimens' substrate. As shown in Fig. 4(b) the major phases on H X alloy after 10 days immersion are Ni2.9Cr0.7Fe0.36, $MgCr_2O_4$, $NiFe_2O_4$ and NiO, which is same to the major phase on H X alloy after 21 days immersion. No protective Cr_2O_3 or Fe_xO_y is identified on the surface of In625 and H X alloys.

Since the experiments were conducted in air atmosphere, the water vapor in the air can permeate into the molten salt and result in high temperature hydrolysis of $MgCl_2$:

$$MgCl_2 + H_2O \rightarrow MgO + 2HCl\uparrow \quad (3)$$

$MgCr_2O_4$ and $NiFe_2O_4$ may be formed as the following reactions:

$$Cr_2O_3 + MgO \rightarrow MgCr_2O_4 \quad (4)$$

$$NiO + Fe_2O_3 \rightarrow NiFe_2O_4 \quad (5)$$

The phase of Cr_2O_3 is not detected on the surface of In625 and H X alloy after 5, 10 and 21 days immersion. This indicates that the oxide scale of Cr_2O_3 formed on the surface of specimens is too thin at the initial stage and it reacts with other oxides to form a new phase after 10 days immersion. In addition, no diffraction peaks representing Mo or Fe oxides were detected on the surface of In625 and H X alloy. They may be dissolved in the immersion medium or removed during ultrasonic washing. It have been reported that iron oxides have a faster dissolution rate than chromium oxides in the chloride molten salts [21].

For H B-3 alloy, the major phase on the surface is detected to be $MoNi_4$ after 5, 10 and 21 days immersion. No corrosion products XRD peaks were detected on the surface. This indicates that small amount of corrosion products formed on the surface of the alloy, or the formed products do not crystallize.

Since the corrosion products are washed before XRD analysis and metal chlorides may be dissolved as well, they are not identified.

The cross-sectional SEM images of the In625, H X and H B-3 alloys corrode for 21 days at 600 °C in molten NaCl-$CaCl_2$-$MgCl_2$ in the air are shown in Fig. 5(a), (b), and (c). It is found from Fig. 5(a), (b) that both of the cross-sectional SEM micrographs of In625 and H X alloys clearly reveal a three-layered structure: outer corrosion layer, inner corrosion layer and matrix.

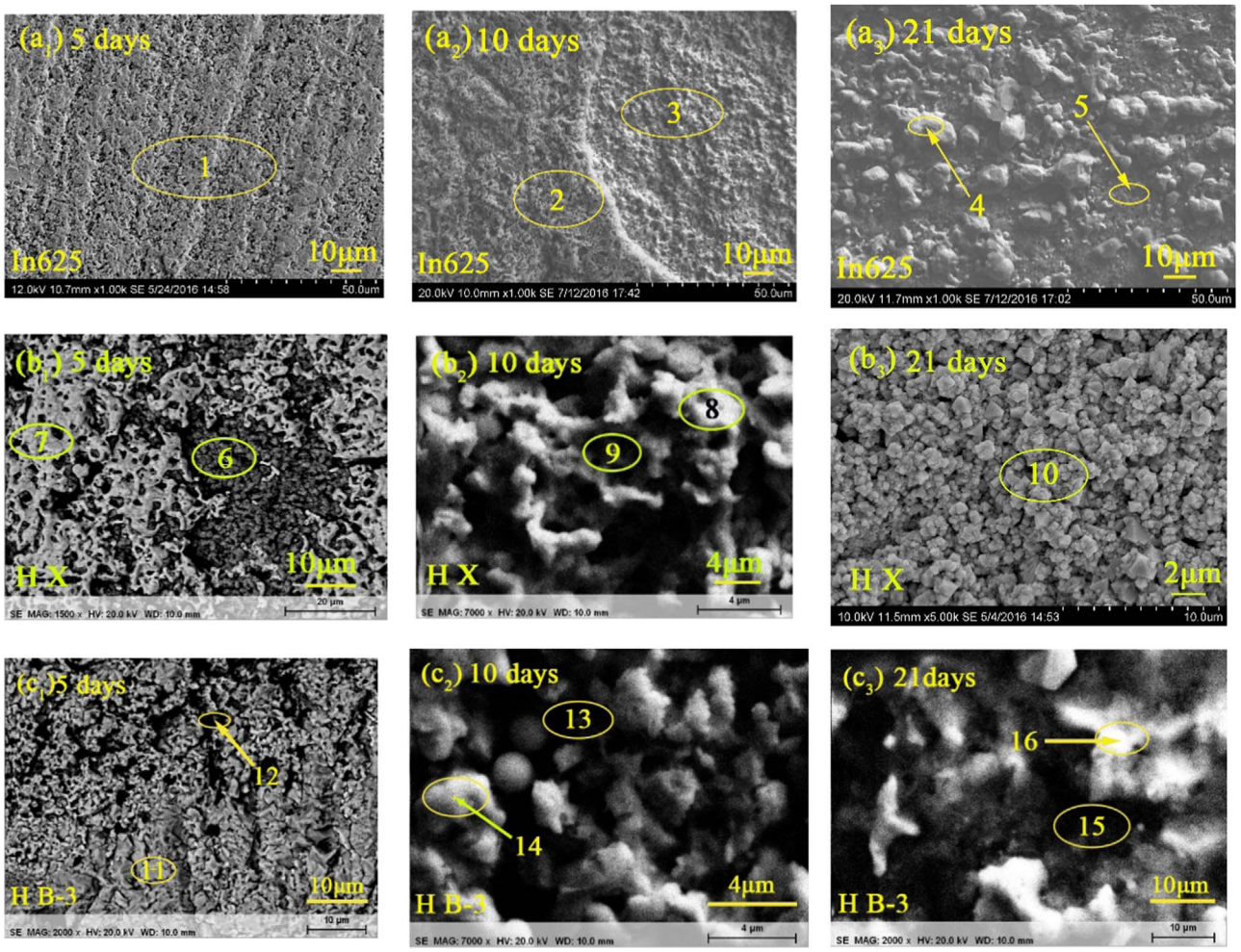

Fig. 3. Scanning electron micrographs of specimens after 5(1), 10(2) and 21(3) days immersion: (a) In625, (b) H X and (c) H B-3.

Table 2
Surface EDS analysis of In625, H X and H B-3 alloys specimens after 5, 10, 21 days immersion (At%).

Region	O	Mg	Cr	Fe	Ni	Mo
1	19.68	3.06	5.59	0.64	34.09	4.14
2	55.88	13.93	21.35	-	0.70	1.15
3	7.53	3.22	5.15	0.81	60.81	4.54
4	6.49	0.44	1.11	0.17	43.18	3.12
5	30.39	9.23	11.98	0.30	8.77	1.53
6	45.21	14.15	24.38	0.33	2.70	2.15
7	2.33	0.90	6.45	4.77	58.41	6.81
8	7.85	-	2.75	3.07	53.13	4.61
9	3.67	-	7.17	7.27	64.42	4.95
10	54.75	13.38	19.27	-	0.83	3.56
11	1.44	-	-	-	69.74	9.31
12	6.21	-	1.87	-	71.20	11.27
13	7.55	1.14	0.67	0.48	47.43	6.58
14	20.02	3.91	2.25	0.43	36.90	5.14
15	27.38	5.14	1.89	0.75	7.56	1.51
16	20.02	3.51	0.91	0.36	27.43	4.01

For In625 alloy, the inner corrosion layer (2.5 μm) has many tiny pores. The outer corrosion layer (7.08 μm) is composed of two different color regions which indicates the different elements content. According to the EDS results (Table 3), the bright regions rich in Ni, and the black regions rich in Cr, Mg. Both the corrosion layers remained well adhered to the substrate metal. Obviously, a dense corrosion protective layer (outer corrosion layer) formed on the surface of the specimen. Combined with the element distribution map (Fig. 6), the elements in the outer corrosion layer are mainly O, Cr and Mg. The inner corrosion layer is an obvious Cr-deficient region (Fig. 6). This indicates that Cr has a selective solubility companied with diffusion, reaction and depletion from substrate alloy to molten salt.

For H X alloy, a thin and spallation outer corrosion layer (8.57 μm) was observed on the image which almost has no protective effect for the substrate alloy from further attack by covering the surface of substrate. H X alloy has a much thicker inner corrosion layer (17.4 μm) than In625 alloy (2.5 μm), and the corrosion holes are larger than In625 alloy. The higher Fe content in H X than In625 is to be considered the main reason. The corresponding element distribution map of the cross-sectional is shown in Fig. 7. According to the image, the outer corrosion layer mainly consisted of Ni, O. The junction of the inner and outer corrosion layers is enriched with O, Cr, and Mg where a protective layer which has a corrosion resistance is being generated. Ni, Mo are distributed uniformly in inner corrosion layer. However, compared with matrix, Fe and Cr are depleted in inner corrosion layer. Cr and Fe has a higher diffusion coefficient in $NaCl_2$-$CaCl_2$-$MgCl_2$ molten than Ni and Mo. Cr also has an outward diffusion trend which dissolve from the matrix to form a dense Cr and Mg oxide protective layer ($MgCr_2O_4$) on the alloy surface. To a certain extent, the protective layer can slow down the corrosion.

Fig. 5(c) shows the cross-sectional SEM image of the H B-3 alloy specimens. After 21 days immersion, a corrosion layer with a maximum depth of approximately 15 μm is formed near the surface. It is clear that the substrate of the H B-3 alloy near the corrosion layer is flat and uniform and does not exhibit a porous structure as in In625 and H X alloys. According to the corresponding element distribution map of the

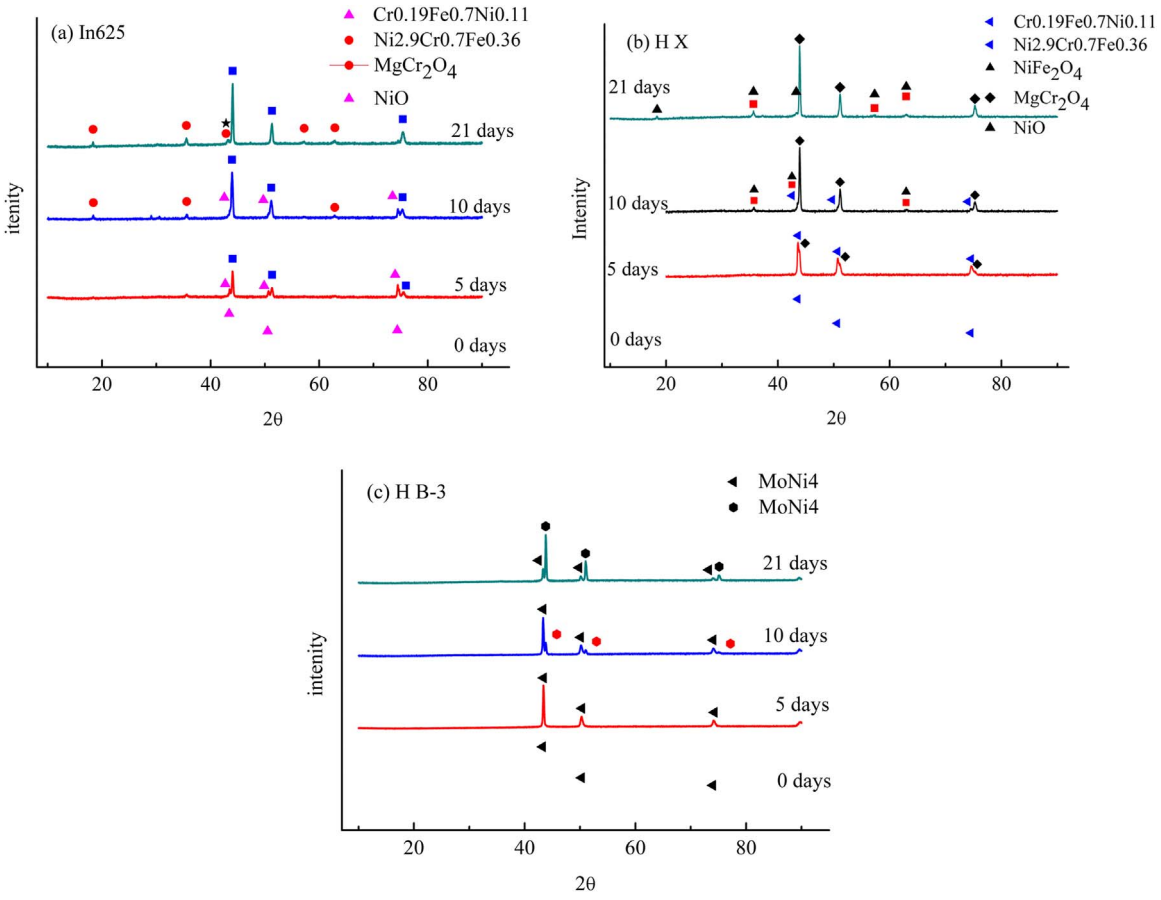

Fig. 4. XRD results of the specimens surfaces after 5, 10 and 21 days immersion at 600 °C: (a) In625, (b) H X, (c) H B-3.

cross-sectional (Fig. 8), Ni and Mo are uniformly distributed in the metal substrate near the corrosion layer. Combined with the surface morphologies (Fig. 3(c)) and EDS analysis results (Table 2) of the specimen, H B-3 shows a uniform corrosion behavior in the NaCl-$CaCl_2$-$MgCl_2$ molten under air. Fig. 3(c) and Fig. 8 indicate that the corrosion reaches equilibrium after immersion for 21 days, which corresponds to the equilibrium in the corrosion dynamic curve.

3.3. Discussion

Previous research shows that the atmospheric air plays a big role in inducing the corrosion in the molten-salt alloy system [12]. The corrosion rate of alloy in molten chloride salt dramatically diminish when the alloy and the salt are isolated from air. Oxygen [11] and water vapor [2] can accelerate the corrosion of the alloy in molten salt. As the experiments are carried out in the air, O_2 and H_2O are the main substances in inducing the corrosion in the molten-salt/alloy systems. Cl_2 and HCl can be present in the molten salt after O_2 and H_2O reacting with Cl^-:

$$4Cl^- + O_2(g) \rightarrow 2O^{2-} + 2Cl_2(g) \quad (6)$$

$$H_2O(g) + 2Cl^- \rightarrow O^{2-} + 2HCl(g) \quad (7)$$

The process of “active oxidation” [22] may be used to explain the formation of NiO and oxides of iron and chromium in the corrosion process. However, a poor Cr region found in the element distribution of cross section of In625 and H X alloys needs to be further explored.

The reason for the formation of the Cr-deficient region in the inner

Table 3
Cross-sectional EDS analyses results of In625 alloy specimens (At%).

Region	O	Fe	Cr	Ni	Mo	Mg
1	18.99	0.61	5.45	66.63	5.34	2.99
2	15.48	2.22	36.1	31.35	5.10	9.81

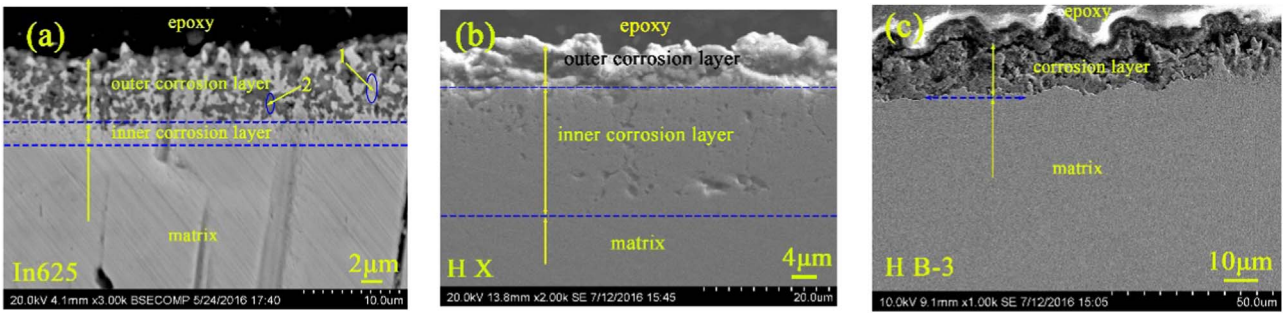

Fig. 5. Cross-sectional SEM photograph of specimens after 21 days immersion at 600 °C: (a) In625, (b) H X, (c) H B-3.

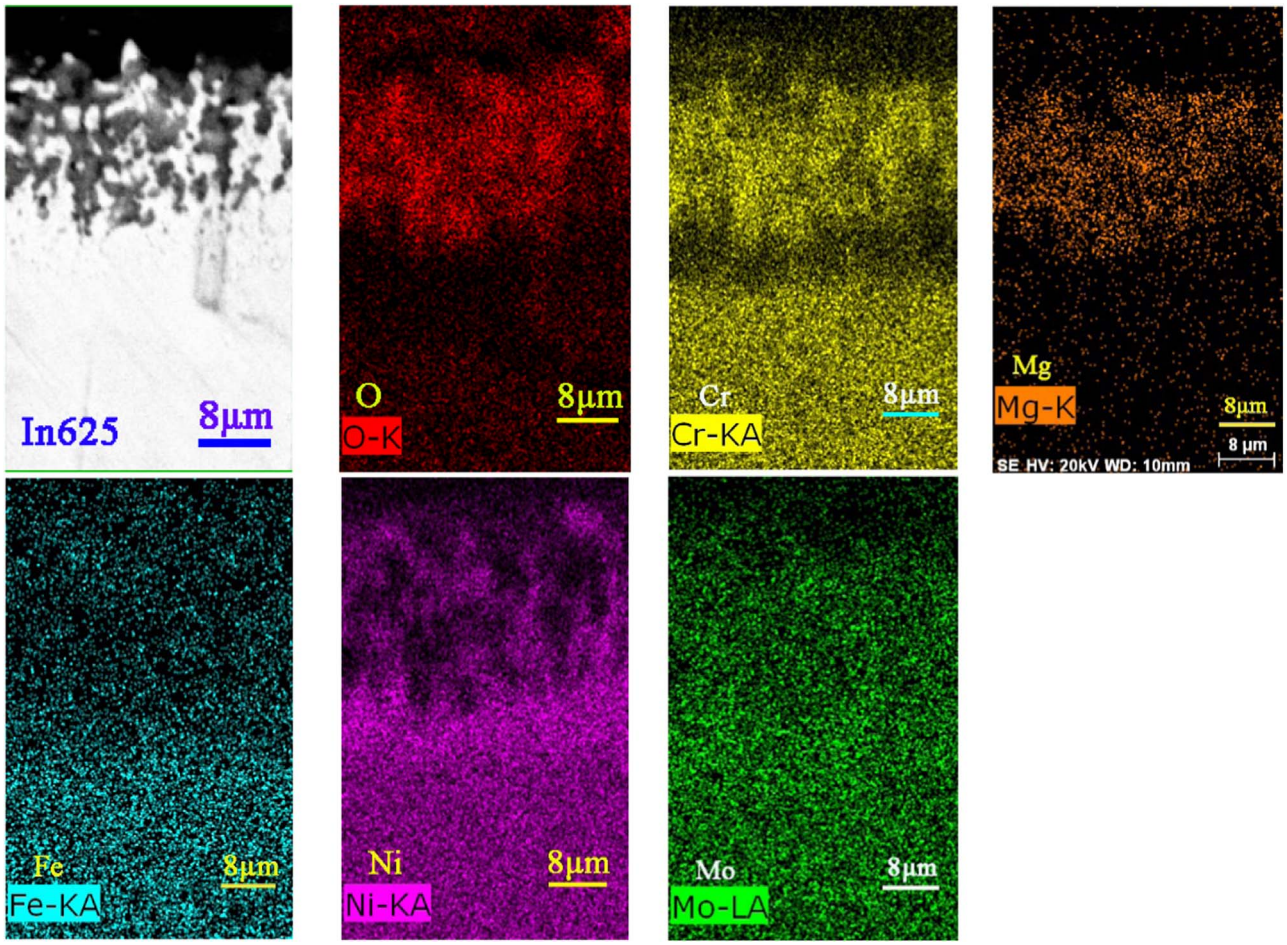

Fig. 6. Cross-sectional SEM image and the elemental distribution of In625 alloy.

corrosion layer of In625 and H X alloy can be explained as follows (shown in Fig. 9). Since the corrosion tests were carried out in air, O_2 and H_2O would partially dissolve in molten NaCl-$CaCl_2$-$MgCl_2$ salt. Simultaneously, $MgCl_2$ is more hydrophilic than NaCl and $CaCl_2$, which lead to the hydrolysis reaction of $MgCl_2{\cdot}nH_2O$ as following equations:

$$MgCl_2(l) + H_2O(g) \rightarrow MgO(s) + 2HCl(g) \quad (8)$$

Thus, not Na_2O and CaO but MgO was detected in the surface and cross section of the samples after corrosion.

The dissolved oxygen would decompose in active adsorbing oxygen due to the high temperature and diffuse towards the alloy surface, and then react with alloys as following equation:

$$xM(s) + (y/2)O_2(g) \rightarrow M_xO_y(s) \quad (9)$$

where M refers to the elements contained in the alloys such as Cr, Ni, Fe and Mo. Besides, O_2 can also react with HCl:

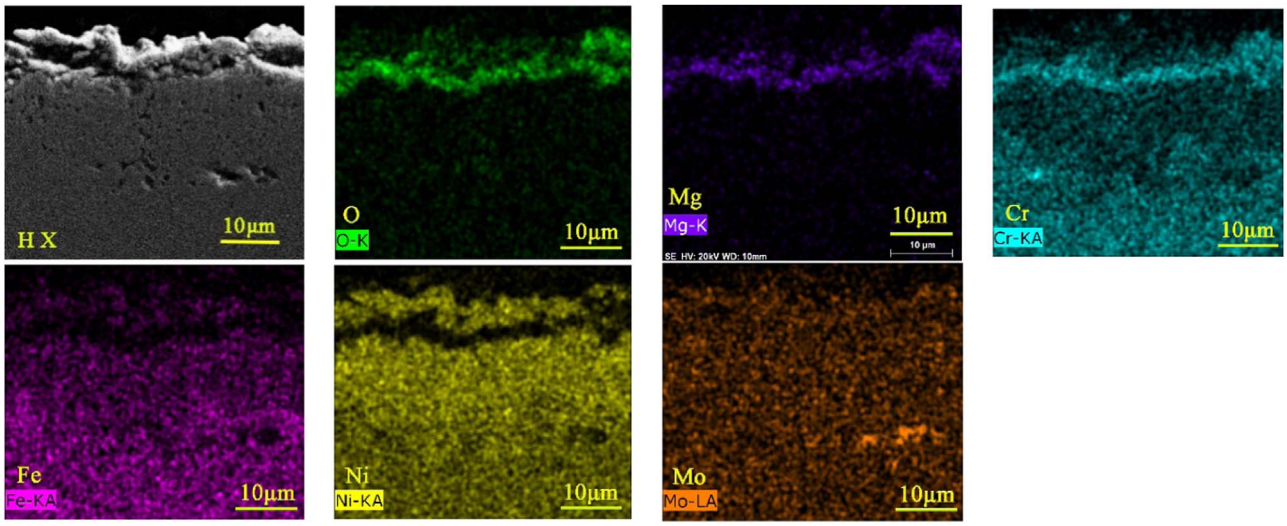

Fig. 7. Cross-sectional SEM image and the elemental distribution of H X alloy.

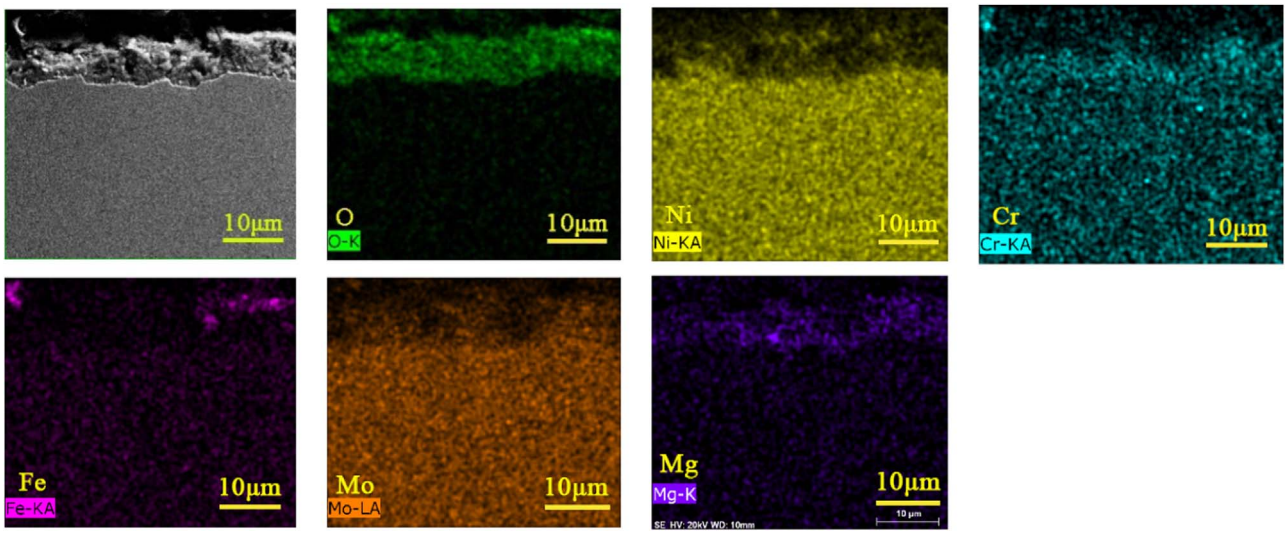

Fig. 8. Cross-sectional SEM image and the elemental distribution of H B-3 alloy.

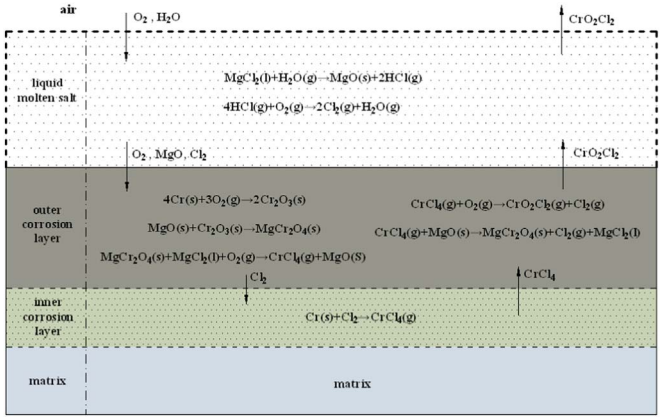

Fig. 9. schematic diagram showing transition of corrosion scales on substrate during hot corrosion in molten salts.

$$4HCl(g) + O_2(g) \rightarrow 2Cl_2(g) + H_2O(g) \quad (10)$$

$$MgO(s) + Cr_2O_3(s) \rightarrow MgCr_2O_4(s) \quad \Delta_r G_m^{\theta}(873K) = -37\ kJ/mol \quad (11)$$

$$2MgCr_2O_4(s) + 8MgCl_2(l) + O_2(g) \rightarrow 4CrCl_4(g) + 10MgO(s) \quad \Delta_r G_m^{\theta}(873K) = -98{\cdot}45\ kJ/mol \quad (12)$$

Cl_2 has the ability to penetrate the protective oxide scale presumably through pores and cracks to react with the substrates, and takes the following reaction:

$$2Cl_2(g) + Cr(s) \rightarrow CrCl_4(g) \quad \Delta_r G_m^{\theta}(873K) = -219.3\ kJ/mol \quad (13)$$

In addition, in the diffusing process of $CrCl_4$ towards the outside, it is oxidized with oxygen and MgO concentration increases with an increasing distance from the alloy surface as the following equations:

$$CrCl_4(g) + O_2(g) \rightarrow CrO_2Cl_2(g) + Cl_2(g) \quad \Delta_r G_m^{\theta}(873K) = -243.6\ kJ/mol \quad (14)$$

Also a part of $CrCl_4$ may react with oxygen as follow:

$$2CrCl_4(g) + 4MgO(s) \rightarrow MgCr_2O_4(s) + 3MgCl_2(l) + Cl_2(g) \quad \Delta_r G_m^{\theta}(873K) = -39.6\ kJ/mol \quad (15)$$

CrO_2Cl_2 and a part of Cl_2 diffuse into the molten salt in the form of gas, the other part of the Cl_2 diffuse to the corrosion layer and alloy substrate to continue the corrosion reactions. Here, the formation of CrO_2Cl_2 requires actual detection.

Chromium has been reported to play an important role in the degradation of alloys in chloride systems [6,7]. The formed dense oxide scale composed of Cr_2O_3, NiO and Fe_3O_4 can provide protection for the substrate alloy from further attack by covering the surface of substrate [10]. However, in this work, the surface protective Cr_2O_3 scale on the surface of In625 and H X alloys may be destroyed after 5 days immersion. The relatively dense corrosion phase formed on the surface of the alloys which has a protective effect for the substrate alloy from further attack by covering the surface of substrate is mainly composed of $MgCr_2O_4$.

As mentioned before, the high Fe content in H X alloy is to be considered the main reason for it has a lower corrosion resistance in molten salt NaCl-$CaCl_2$-$MgCl_2$ at 600 °C than In625 alloy. Figs. 10 and 11 show the Gibbs free energies of chemical reaction between alloy elements and 1 mol O_2 or Cl_2 at different temperatures. It can be seen that the Gibbs free energies of generating iron oxides is close to the Gibbs free energies of the generating chromium oxides, and lower than the Gibbs free energies of generating nickel oxides and molybdenum oxides under 1 mol of O_2. This phenomenon is also suitable for generating metal chlorides of Fe, Cr, Ni and Mo. Therefore, Cr and Fe will be preferentially oxidized and chlorinated compared with Ni and Mo in chloride molten salt. Thus, the thick and porous inner corrosion layer of H X alloy is caused by the preferential deletion of Cr and Fe in specimen.

Combine Figs. 5, 7 and 11, the formation and diffusion of $FeCl_3$ are presumed to be the cause of the formation of the Fe-deficient region in

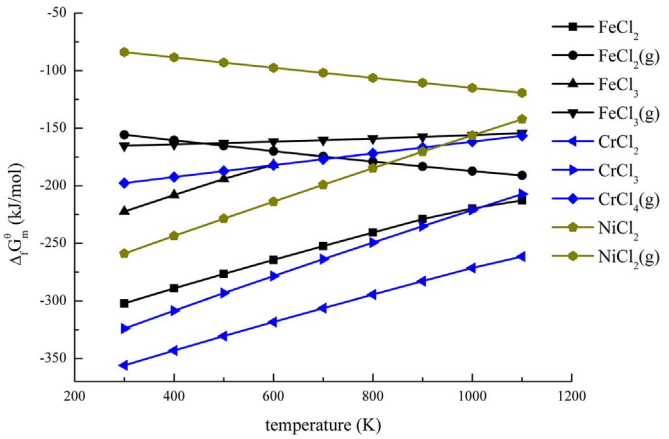

Fig. 10. Gibbs free energies of chemical reaction between alloy elements and 1 mol O_2 at different temperatures.

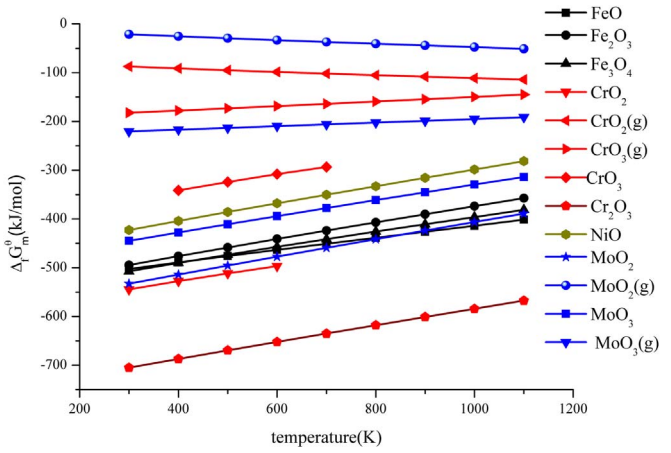

Fig. 11. Gibbs free energies of chemical reaction between alloy elements and 1 mol Cl_2 at different temperatures.

the inner corrosion layer of H X alloy. As we know, the boiling point of $FeCl_3$ only 316 °C [23]. The Fe-deficient region also found in the element distribution of cross section of In625 alloy (Fig. 6). Because the Fe content in In625 alloy is relatively lower than H X alloy (Table 1), In625 alloy shows a the thinner inner corrosion layer than H X alloy. Also, the corrosion holes in the inner corrosion layer are also smaller. Besides, compared with Cr, there is no Fe-rich region detected on the cross section of In625 and H X alloys. In addition to the fact that iron oxides have a faster dissolution rate than chromium oxides in the chloride molten salts [21], the corrosion products formed by Fe are loose and easy fall off into the immersion medium may be another reason.

Ni has been reported has a better corrosion resistance than Cr and Fe in molten chloride salts [4]. Previous research reported that Mo shows resistance to localized corrosion that it can promoted fast re-passivation by forming Mo insoluble compounds [24,25]. However, H B-3 alloy shows higher corrosion rates than In625 and H X alloys, even though H B-3alloy has higher Ni and Mo content. It has been reported that the higher corrosion of Hastelloy N in molten salt NaCl-KCl-$ZnCl_2$ is mainly due to its low Cr content (7%) [8]. Thus, we believe the low Cr content (2.13%) also the main reason for H B-3 alloy has a higher corrosion rates in molten salt NaCl-$CaCl_2$-$MgCl_2$. As shown in Figs. 3, 5 and 8, there is no relatively dense corrosion layer formed on the surface of H B-3 alloy. The corrosion of the immersion medium to the alloy is continuous. As seen in Fig. 8, Mo and Ni are distributed evenly in the alloy substrate near the corrosion layer. According to Figs. 10 and 11, compared with Cr and Fe, the Gibbs free energies of generating molybdenum oxides is more close to the Gibbs free energies of generating nickel oxides. Thus, they are uniformly reduced on the surface of the alloy with the progress of corrosion.

Besides, the preferential dissolution of MoO_x can consumes oxygen and inhibits the dissolution of NiO [10], this enhanced the corrosion resistance of the alloy to some extent. It can be inferred that in this work the diffusion rate of nickel, molybdenum and their corrosion products controlled the corrosion rate of H B-3. Although, the activity of metals in chloride salt decrease in the order [26]: Cr > Fe > Co > Ni > Mo, Inconel 625 and H astelloy X show a better corrosion resistance than Hastelloy B-3 alloy. The test shows that a certain amount of Cr content can improve the corrosion resistance of Nickel-based alloys in chloride molten salt which is consistent with the previous research of Cr is one of the main alloying elements ensuring better corrosion resistance of Hastelloy series [10].

4. Conclusions

Inconel 625, Hastelloy X and Hastelloy B-3 alloys were selected for the corrosion tests in molten salt NaCl-$CaCl_2$-$MgCl_2$ by immersion for up to 21 days at 600 °C in the presence of air. Inconel 625 alloy shows resist corrosion better than Hastelloy X and Hastelloy B-3 alloys in molten NaCl-$CaCl_2$-$MgCl_2$ salt.

For Inconel 625 and Hastelloy X alloys, the outward diffusion of $CrCl_4$(g) generated by chromium and Cl_2 lead to the poor Cr zone in the inner corrosion layer. $MgCr_2O_4$ attached to the alloy surface formed a compact protective layer and thus resist corrosion better.

The higher content of Fe in Hastelloy X alloy makes it suffer a higher corrosion in molten salt NaCl-$CaCl_2$-$MgCl_2$ than Inconel 625 alloy. In addition to Cr, Fe in the alloys also has the preferential solubility in the molten salt NaCl-$CaCl_2$-$MgCl_2$. However, under the experimental conditions, it is almost impossible to form a protective corrosion layer.

Uniform corrosion occurred in Hastelloy B-3 alloy in NaCl-$CaCl_2$-$MgCl_2$ molten salt. The corrosion rate of Ni and Mo determines the corrosion rate of alloy.

Ni and Mo in nickel-based alloys showed higher stability in the corrosion test, but the addition of Cr in the nickel-based alloys improved the corrosion resistance of the alloy.

Acknowledgements

This work was supported by the National Natural Science Foundation of China (No. U 1507113), The key projects of National Natural Science Foundation of China (51436009), the National Natural Science Foundation of China (No. 51376067).

References

[1] J.C. Gomez-Vidal, R. Tirawat, Corrosion of alloys in a chloride molten salt (NaCl-LiCl) for solar thermal technologies, Sol. Energy Mater. Sol. Cells 157 (2016) 234–244.
[2] P.D. Myers, D.Y. Goswami, Thermal energy storage using chloride salts and their eutectics, Appl. Therm. Eng. 109 (2016) 889–900.
[3] X.L. Wei, M. Song, W.L. Wang, J. Ding, J.P. Yang, Design and thermal properties of a novel ternary chloride eutectics for high-temperature solar energy storage, Appl. Energy 156 (2015) 306–310.
[4] J.W. Wang, C.Z. Zhang, Z.H. Li, H.X. Zhou, J.X. He, J.C. Yu, Corrosion behavior of nickel-based supperalloys in thermal storage medium of molten eutectic NaCl-$MgCl_2$ in atmosphere, Sol. Energy Mater. Sol. Cells 164 (2017) 146–155.
[5] M.S. Sohal, M.A. Ebner, P. Sabhar, Engineering database of liquid salt thermo-physical, Technical Report, 2010.
[6] Y.S. Li, M. Spiegel, S. Shimada, Corrosion behaviour of various model alloys with NaCl-KCl coating, Mater. Chem. Phys. 93 (2005) 217–223.
[7] T. Ishitsuka, K. Nose, Stability of protective oxide films in waste incineration environment – solubility measurement of oxides in molten chlorides, Corros. Sci. 44 (2002) 247–263.
[8] K. Vignarooban, P. Pugazhendhi, C. Tucker, D. Gervasio, A.M. Kannan, Corrosion resistance of Hastelloys in molten metal-chloride heat-transfer fluids for concentrating solar power applications, Sol. Energy 103 (2014) 62–69.
[9] G.Y. Lai, Molten salt corrosion, in: High-Temperature Corrosion and Materials Applications, ASM International, Chapter15, 2007, pp. 409–421.
[10] S.N. Liu, Z.D. Liu, Y.T. Wang, J. Tang, A comparative study on the high temperature corrosion of TP347H stainless steel, C22 alloy and laser-cladding C22 coating in molten chloride salts, Corros. Sci. 83 (2014) 396–408.
[11] A. Rahmel, Corrosion, in: D.G. Lovering (Ed.), Molten Salt Technology, Plenum Press, New York, 1982, pp. 265–283.
[12] K. Vignarooban, X.H. Xu, K. Wang, E.E. Molina, P. Li, D. Gervasio, A.M. Kannan, Vapor pressure and corrosivity of ternary metal-chloride molten-salt based heat transfer fluids for use in concentrating solar power systems, Appl. Energy 159 (2015) 206–213.
[13] D.L. Wu, S.M. Jiang, Q.X. Fan, J. Gong, C. Sun, Hot Corrosion Behavior of a Cr-Modified Aluminide Coating on a Ni-Based Superalloy, Acta Metall. Sin.-Engl. 27 (2014) 627–634.
[14] X.M. Lou, W.R. Sun, S.R. Guo, Z.Q. Hu, Hot corrosion behavior of IN718 alloy and its effect on mechanical properties, Rare Metal. Mater. Eng. 37 (2008) 259–263.
[15] Z. Lei, M.C. Zhang, J.X. Dong, Hot corrosion behavior of powder metallurgy Rene95 nickel-based superalloy in molten NaCl-Na_2SO_4 salts, Mater. Des. 32 (2011) 1981–1989.
[16] ASTM Standards: G1-03 practice for preparing, cleaning, and evaluating corrosion test specimens, the ASTM website, ⟨www.astm.org⟩, 2011.
[17] A.G. Fernandez, F.J. Perez, Improvement of the corrosion properties in ternary molten nitrate salts for direct energy storage in CSP plants, Sol. Energy 134 (2016) 468–478.
[18] A.S. Dorcheh, R.N. Durham, M.C. Galetz, Corrosion behavior of stainless and low-chromium steels and IN625 in molten nitrate salts at 600 °C, Sol. Energy Mater. Sol. Cells 144 (2016) 109–116.

[19] A.S. Dorcheh, R.N. Durham, M.C. Galetz, Corrosion behavior of stainless and low-chromium steels and IN625 in molten nitrate salts at 600 °C, Sol. Energy Mater. Sol. Cells 144 (2016) 109–116.
[20] M. Liu, J.Y. Zheng, Y.L. Lu, Z.J. Li, Y. Zou, X.H. Yu, X.T. Zhou, Investigation on corrosion behavior of Ni-based alloys in molten fluoride salt using synchrotron radiation techniques, J. Nucl. Mater. 440 (2013) 124–128.
[21] Y. Kawahara, High temperature corrosion mechanisms and effect of alloying elements for materials used in waste incineration environment, Corros. Sci. 44 (2002) 223–245.
[22] M. Hofmeister, L. Klein, H. Miran, R. Rettig, S. Virtanen, R.F. Singer, Corrosion behaviour of stainless steels and a single crystal superalloy in a ternary LiCl-KCl-CsCl molten salt, Corros. Sci. 90 (2015) 46–53.
[23] R. David, Handbook of Chemistry and Physics, (the 84th), CRC Press, 2003, pp. 4-39–4-93.
[24] P. Jakupi, J.J. Noel, D.W. Shoesmith, The evolution of crevice corrosion damage on the Ni-Cr-Mo-W alloy-22 determined by confocal laser scanning microscopy, Corros. Sci. 54 (2012) 260–269.
[25] A. Pardo, M.C. Merino, A.E. Coy, F. Viejo, R. Arrabal, E. Matykina, Pitting corrosion behaviour of austenitic stainless steels-combining effects of Mn and Mo additions, Corros. Sci. 50 (6) (2008) 1796–1806.
[26] J. Ambrosek, Molten chloride salts for heat transfer in nuclear systems, Preliminary Proposal for Ph.D. Dissertation, University of Wisconsin, Madison, WI, 2010.